ELSEVIER

Journal of Power Sources 113 (2003) 157–165

JOURNAL OF POWER SOURCES

www.elsevier.com/locate/jpowsour

Anthracite as a candidate for lithium ion battery anode

Young-Jun Kim, Hojung Yang, Seong-Ho Yoon, Yozo Korai, Isao Mochida*, Cha-Hun Ku

Institute of Advanced Material Study, Kyushu University, Kasugakoen, Kasuga, Fukuoka 816-8580, Japan

Received 1 July 2002; received in revised form 9 September 2002; accepted 24 September 2002

Abstract

Four kinds of anthracites from different regions were investigated as anodic materials of Li ion secondary battery by varying their calcination temperatures. Hon-gye anthracite calcined at 1000–1150 °C showed a high reversible capacity at low potential region of 0–0.12 V, which is typical with hard carbon. The highest capacity of 370 mAh/g was obtained with the Hon-gye among anthracites calcined at 1100 °C. The graphitization started with the anthracite above 1600 °C to provide capacity at ca. 0.2 V which reflects the intercalation of graphitic carbon. The anthracite calcined at 1000–1150 °C was indicated to carry the largest d_{002} and smallest Lc(002). And TEM observation showed micropores among the graphite clusters. The large capacity of the anthracite as hard carbon is ascribed to its many micropores among the smallest graphite units which can accommodate highly reduced lithium ions.

Keywords: Anthracite; Coking; Transmission electron microscopy; X-ray diffraction; Electrochemical properties

1. Introduction

Various carbon materials have been investigated as the potential anode for lithium ion secondary battery to find a higher energy density, higher efficiency and longer cycle life [1–15]. Non-graphitizable carbons attract much attention as a candidate of next generation among the carbon materials because they provide a higher discharge capacity near 0 V and rapid charge–discharge. These materials are distinguished from the graphitic carbons in terms of the lower degree of crystallinity but the higher degree of microporosity [2,3,5–10,13,16,17]. It is generally accepted that Li^+ storage sites in non-graphitizable carbons are very different from those of graphitizable carbons. Several models of sites to explain the reversible storage sites in non-graphitizable carbons for lithium such as pores and voids among single layers or crimped carbon sheets have been proposed [5,16,18–20]. However, it is a problem to obtain high charge density per volume of such carbons.

Coals of various ranks can provide a series of coke, of which graphitic structure and properties vary continuously, reflecting their rank or softening behaviors. Dahn and co-workers [21] have reported the anodic behavior of coke derived from various coals, suggesting that the high volatile bituminous coal is most useful for giving the best performance non-graphitizable carbon because of its smallest fraction of stacked graphene sheets and the largest number of nanoscopic pores. It was reported that the coke from lower rank coals exhibited a larger capacity per weight due to more voids among smaller graphene clusters, whereas its very low density due to its lower coking value reduced the capacity per volume [22]. Low coulombic efficiency for the first cycle is another problem. The pressurized carbonization increased the reversible capacity per volume, increasing the density of the coke. Higher ranking coals provided graphite-like behaviors as anodic materials when heat-treated at higher temperature. The density of the coke was fairly higher in comparison with coke from lower ranking coals. However, there is no rule of thumb so far.

Among a wide range of coals, anthracite is interesting for its abundance, low cost, high carbon content, non-graphitizable nature, microporous structure and high density [23–28]. Easy handling and simple material preparation make the anthracite attractive as a candidate for the anode. The anthracite is known to behave like hard carbons by the heat-treatment below 2000 °C and become soft carbons above 2500 °C. Franklin [29] suggested that most of the anthracites show preferred orientation of their carbon layers parallel to the bedding plane by observing X-ray diffraction patterns. Nevertheless, they are not graphitized below 2000 °C and show a similar small scale porosity as other

* Corresponding author. Tel.: +81-92-583-7797; fax: +81-92-583-7798.
E-mail address: mochida@cm.kyushu-u.ac.jp (I. Mochida).

0378-7753/02/$ – see front matter
PII: S0378-7753(02)00528-1

hard carbons do. Oberlin and Terriere [30] showed by TEM observation that flattening of the pores, which are not present in hard carbons, occurs in anthracites and that this flattening induces a preferred orientation of the carbon planes above 1700 °C, which in turn allows graphitization. The high ranking of the anthracite promises a high coke yield and low oxygen contents. Ash minerals in the anthracite must be dealt with since they reduce the carbon content and may react with lithium.

In this study, four kinds of anthracites were selected to investigate anodic performances of their coke calcined at various temperatures. Their high coke yield, high density and low oxygen content are most attractive for anodic materials in addition to their microporosity without macropores. Low oxygen content is expected to improve the first cycle efficiency. Anodic performance of anthracite was correlated with its structure investigated by TEM.

2. Experimental

2.1. Materials

Four anthracites from Vietnam (Hon-gye), China, South Korea, and Spain were used in the present study. Their compositions of as-received forms are summarized in Table 1. XRD analyses of anthracites and their coke were carried out on a Rigaku instrument using Cu Kα radiation, a 0.02° step size and 2°/min scan rate. Their nanostructure and morphology were examined using a high resolution transmission electron microscope (JEOL JEM-2001).

2.2. Heat-treatment

After grinding and sieving (<45 μm), anthracite coals were carbonized in a Pyrex glass tube at 600 °C for 1 h under nitrogen flow at a heating rate of 1 °C/min. The semi-coke was further calcined at 900–1800 °C for 1 h under argon flow by a heating rate of 10 °C/min.

2.3. Cell fabrication and electrochemical measurements

Test electrode was fabricated by mixing active material with 10 wt.% poly(vinylidene fluoride) (PVDF) binder in 1-methyl-2-pyrrolidone (NMP) solution. The slurry was coated on copper foil and then vacuum dried for 6 h at 120 °C. The test electrode was assembled in a typical two-electrode test cell using lithium foil as the counter electrode, 1 M $LiPF_6$ in EC/DEC (1:1, v/v) as the electrolyte, and microporous polypropylene as the separator. The cell assembly was carried out in an argon-filled glove box.

Table 1
Elemental analysis of anthracite coals (wt.%)

Anthracite	Source	C	H	N	Ash
Hon-gye	Vietnam	79.87	2.89	1.45	11.6
Shan-xi	China	80.85	1.13	0.35	12.5
South Korea	South Korea	61.61	1.15	0.36	24.6

Electrochemical measurement was performed using two types of charge and discharge methods. The first was a constant current method (CC), where charge and discharge were carried out at a specific constant current of 10 mA/g between lower target voltage and upper cut-off voltage of 2.0 V versus Li/Li^+. The other was a constant current and constant voltage charge method, where the charge was carried out first to 0 V by a constant current (30 mA/g) and then held at 0 V for 6 h, while the same discharge method (constant current: 30 mA/g) was applied. Differential capacity plot (dcp) was obtained by differentiating the discharge profiles.

3. Results

3.1. Structural change of Hon-gye anthracite by heat-treatment

Fig. 1 illustrates the weight change of Hon-gye anthracite and its first differential derivative by the thermal gravimetric analysis. The volatile components of the Hon-gye anthracite were largely removed at 400–500 °C where coking occurred. Small weight loss evolving H_2 and CH_4 continued above this temperature range.

Fig. 2 shows the change of H/C ratio and ash content according to HTT, calculated from elemental analyses. The H/C ratio decreased largely up to 1000 °C and then slowly. Ash content decreased from 12 to 7% according to HTT. Anthracite calcined at 1000 °C showed ash content of 9% and H/C = 0.07.

X-ray diffraction patterns of as-received and heat-treated Hon-gye anthracites are illustrated in Fig. 3. As-received coal showed a rather narrow peak at $2\theta = 25°$. The peak was broadened, shifting to a lower angle by the heat-treatment up

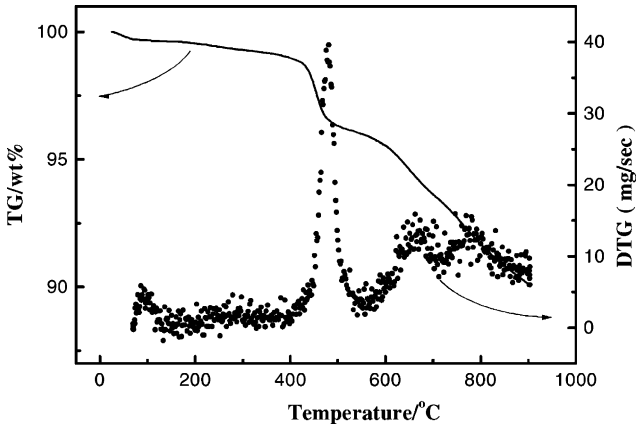

Fig. 1. Thermal gravimetric analysis of as-received Hon-gye anthracite (heating rate: 10 °C/min).

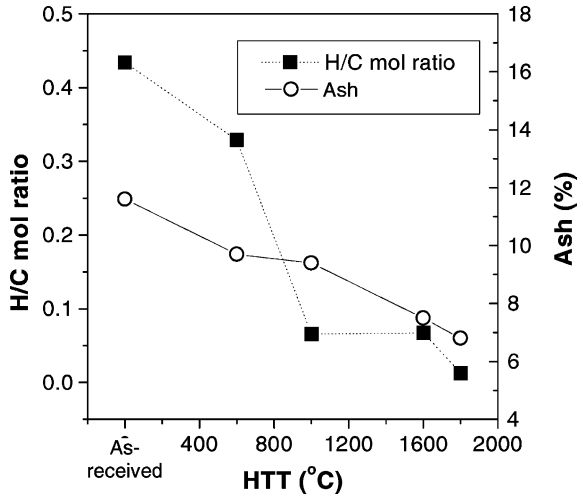

Fig. 2. Elemental analysis of Hon-gye anthracite calcined at various temperatures.

to 1000 °C. The peak was moderately sharpened to 1200 °C, maintaining the diffraction angle. Heat-treatment above 1600 °C sharpened and shifted the peak to 26.5°. According to the XRD patterns, the graphitization started above 1600 °C.

3.2. Anodic behaviors of heat-treated Hon-gye anthracite

Hon-gye anthracite showed unique discharge profiles, reflecting the calcination temperatures as shown in Fig. 4.

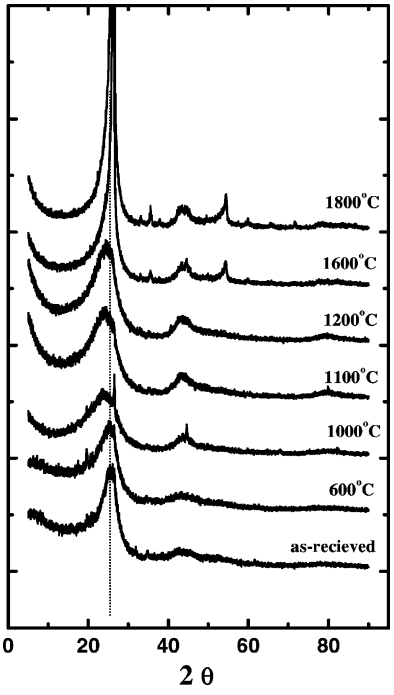

Fig. 3. Powder X-ray diffraction patterns of Hon-gye anthracite.

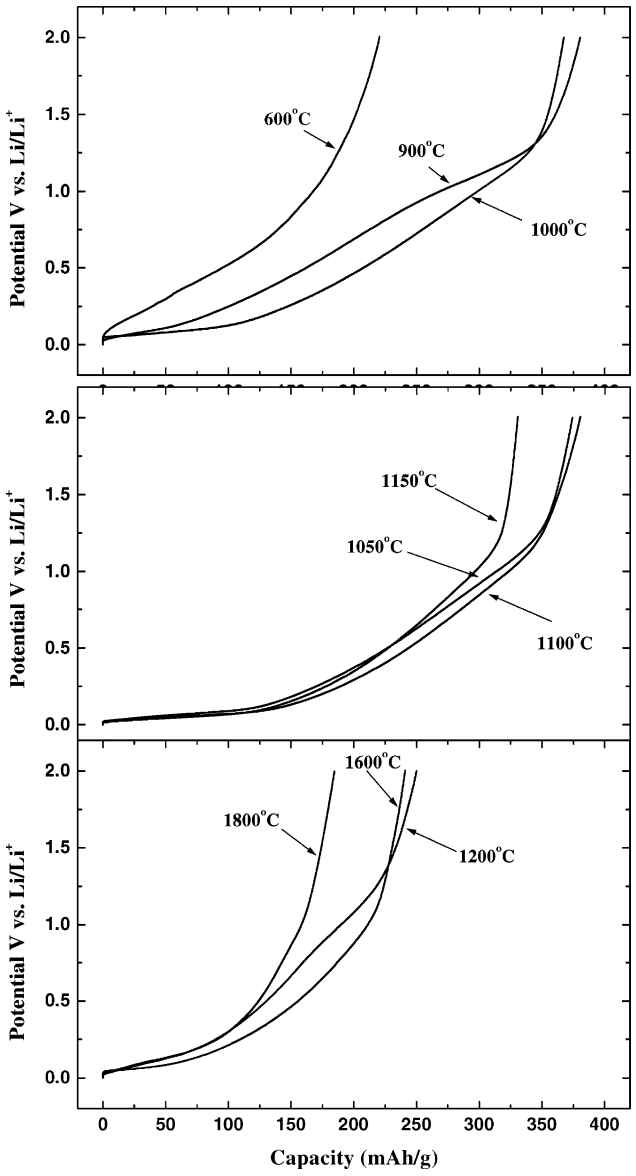

Fig. 4. Discharge profiles of Hon-gye calcined at various temperatures, CCCV (charge: 30 mA/g to 0 V and at 0 V for 6 h, discharge: 30 mA/g to 2 V).

Three types of profiles were observed according to HTT. Anthracite calcined at 900 °C showed discharge capacities at ca. 0.1 V and at an increasing potential from 0.1 to 0.8 V, where a plateau discharge was observed. Its total capacity was 380 mAh/g to be similar to that of heat-treated at 1100 °C, although their discharge capacities at the respective potential regions were very different.

The profile of anthracite calcined at 1000–1150 °C exhibited a plateau at ca. 0.1 V reflecting deinsertion of lithium ion, and a considerable discharge at increasing potential from 0.1 to 0.8 V, first slowly and then sharply. Plateau at ca. 0.8 V was not observed. Capacity increased with HTT and reached the maximum value of about 370 mAh/g at 1100 °C due to the largest capacity in a low potential region (0–0.1 V). The capacity decreased above 1100 °C.

The anthracite calcined at 1800 °C showed a small plateau at 0–0.25 V where the potential started to increase slowly as typical graphite.

Fig. 5 shows the collected charge–discharge profiles of Hon-gye anthracite heat-treated at 900 and 1100 °C. Different charging methods by constant current (CC) and constant current and constant voltage (CCCV) were compared. The anthracite heated at 900 °C provided a discharge with increasing potential from 0.1 to 1.25 V by CC charge. When CCCV inserted Li ion at 0.1–0 V, discharge at 0–0.1 and 1–1.5 V was observed. Such discharge profiles were reported characteristic to hard and soft carbons, respectively [13,16,17,31,32]. When charged at 0.1–0 V by CCCV, the anthracite calcined at 900 °C showed 80 mAh/g and that calcined at 1100 °C showed 140 mAh/g up to 0.1 V. The anthracite heated at 1100 °C showed a plateau at 0–0.1 V. It showed no plateau by only CC charge such as the anthracite heated at 900 °C.

Fig. 6 shows the differential capacity versus potential of the anthracite calcined at 900–1800 °C. Different discharge potentials due to the calcination temperatures were definitely illustrated in this figure. The anthracite calcined at 900 °C showed peaks at 0.05 and 1.06 V, while those at 1000–1200 °C showed a single peak at 0.05 V. The anthracite calcined at 1600–1800 °C showed peaks at 0.05, 0.12 and 0.16 V.

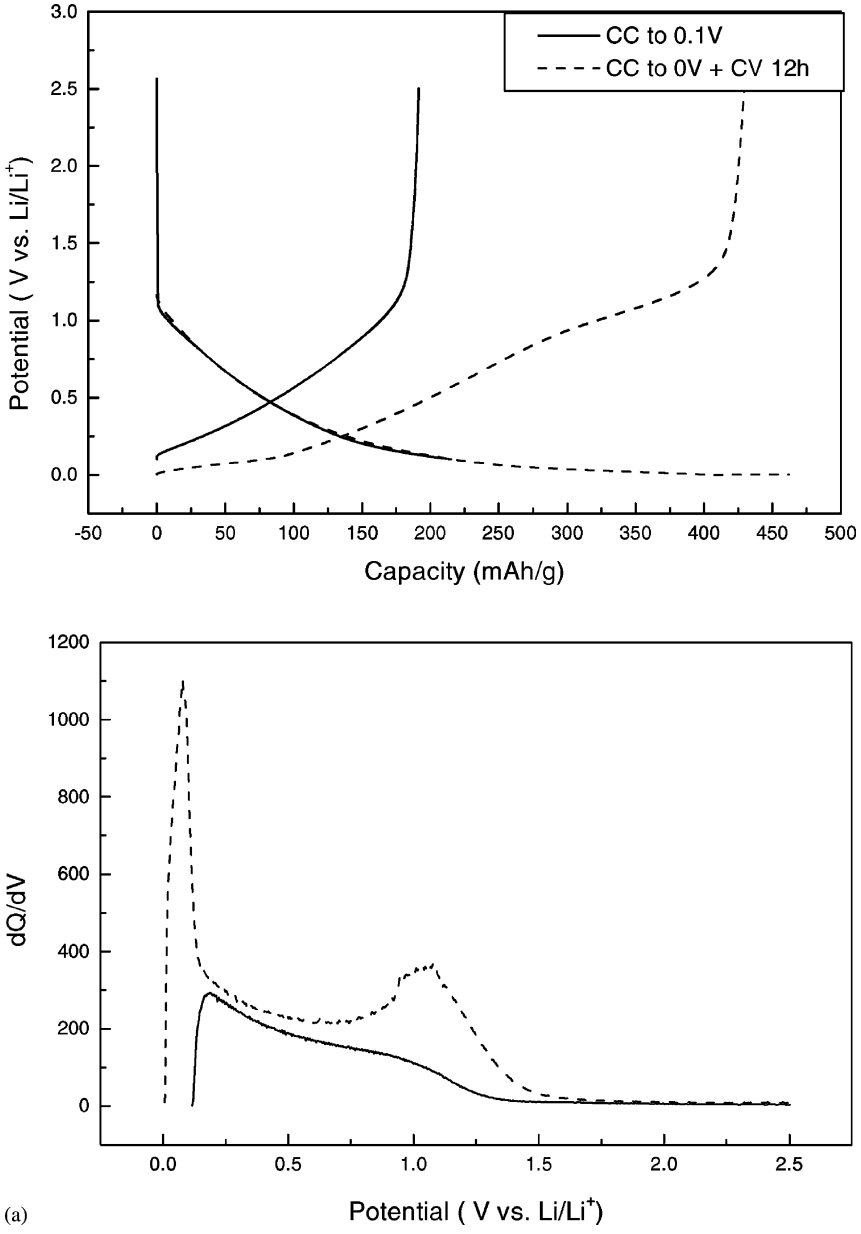

Fig. 5. Charge–discharge profiles of Hon-gye, solid line: CC (10 mA/g charge to 0.1 V and 10 mA/g discharge), dotted line: CC–CV (30 mA/g charge OCV–0 V and 30 mA/g discharge) (a) HTT = 900 °C (b) HTT = 1100 °C.

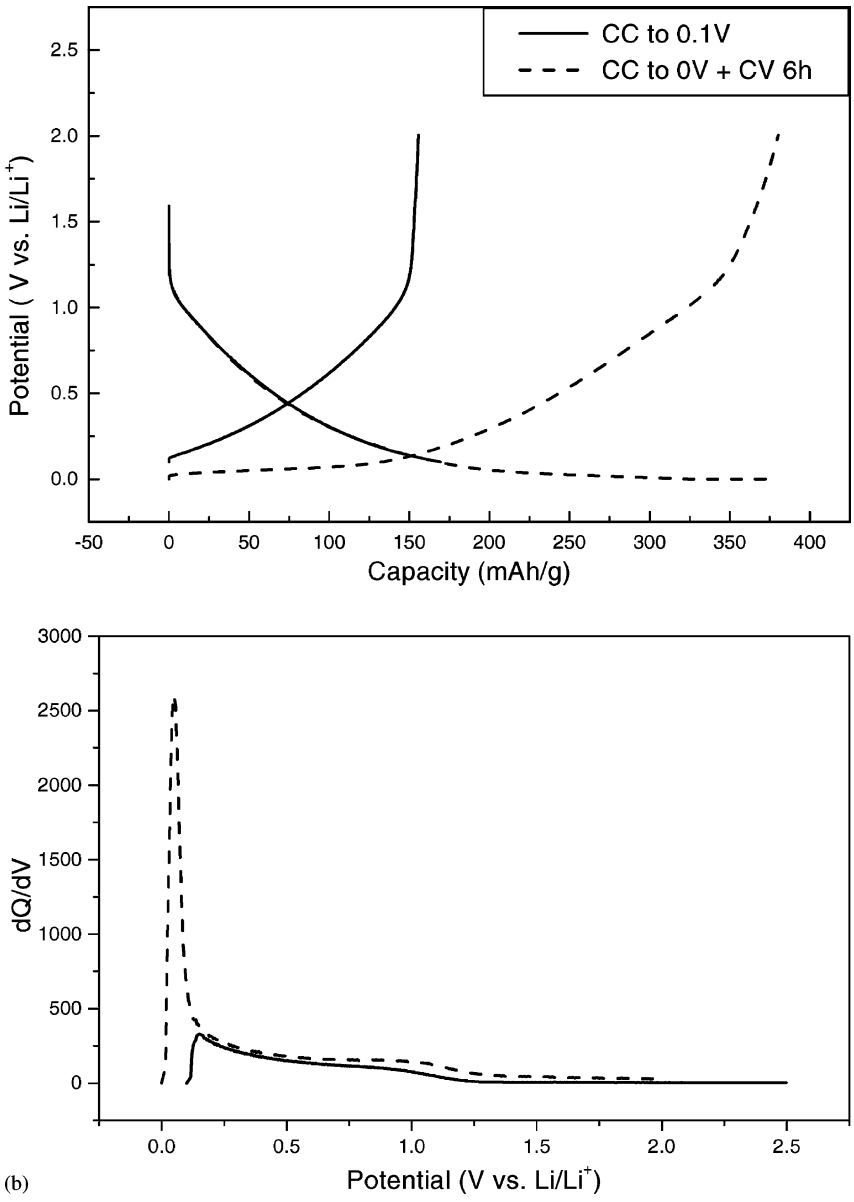

Fig. 5. (*Continued*).

Thus, significant differences of discharge potentials were observed over the anthracite heated at 900–1800 °C. A small peak at 1.06 V which was observed with the anthracite heated at 900 °C, disappeared above 1000 °C. The peak located at 0.05 V became markedly emphasized as the calcination temperature was raised to 1100 °C. Such behaviors are typically observed with a hard carbon. Calcination at 1200 °C reduced the intensity of the peak at 0.05 V.

The three continuous peaks of discharge characteristics to the staged discharge of graphite electrode changed their relative intensities, reflecting the graphitization extent.

Regardless of calcination temperature, Hon-gye cokes retained reversible capacity up to 20 cycles, as shown in Fig. 7. Such good cycle retention of the particular anthracite must be noted.

3.3. Anodic performance and XRD profiles of other anthracite coals

Fig. 8 shows charge–discharge profiles and differential peaks of discharge of several anthracites heated at 1100 °C from different production regions. The reversible capacity increased in the order of South Korea, China, Spain and Hon-gye. Three anthracites calcined at 1100 °C showed similar profiles of discharge plateau at 0.1 V, gradual increase of discharge potential to 1.25 V and rapid increase of potential, whereas South Korea anthracite showed a very

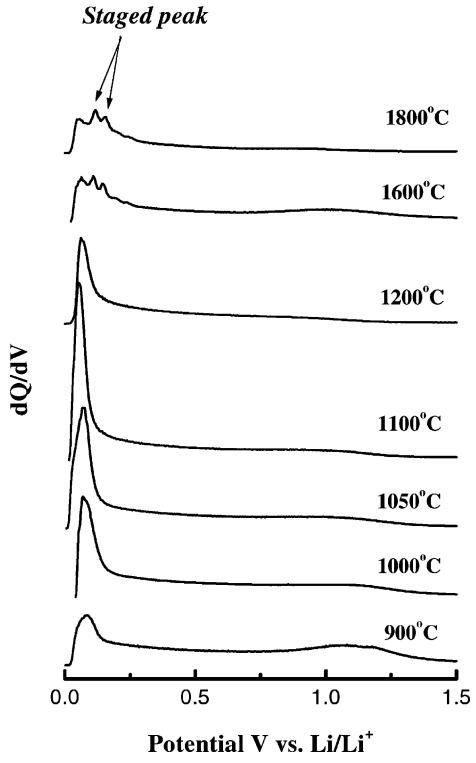

Fig. 6. Differential capacity plots of Hon-gye anthracite.

little plateau. Hon-gye, China, and South Korea anthracites showed 86, 49 and 17 mAh/g of plateau discharge, respectively. Very large capacity at this potential range of Hon-gye anthracite must be noted.

Fig. 9(a) shows the XRD patterns of as-received Hon-gye and other anthracites. Compared to Hon-gye anthracite, China and South Korea anthracites showed many sharp peaks in addition to carbon peak, indicating a quantity of

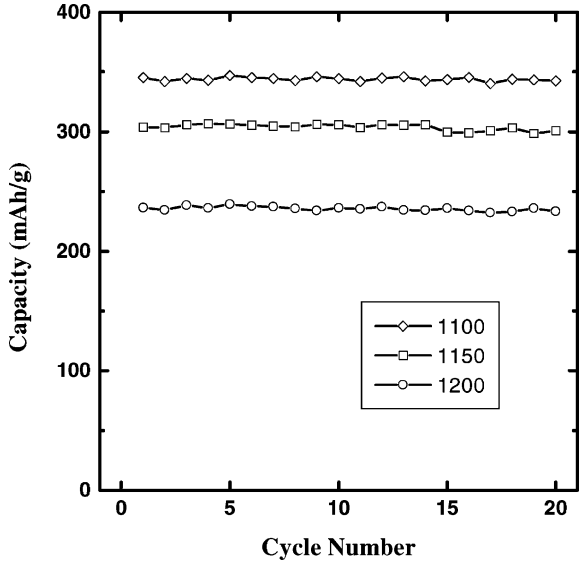

Fig. 7. Cycle behaviors of Hon-gye anthracite.

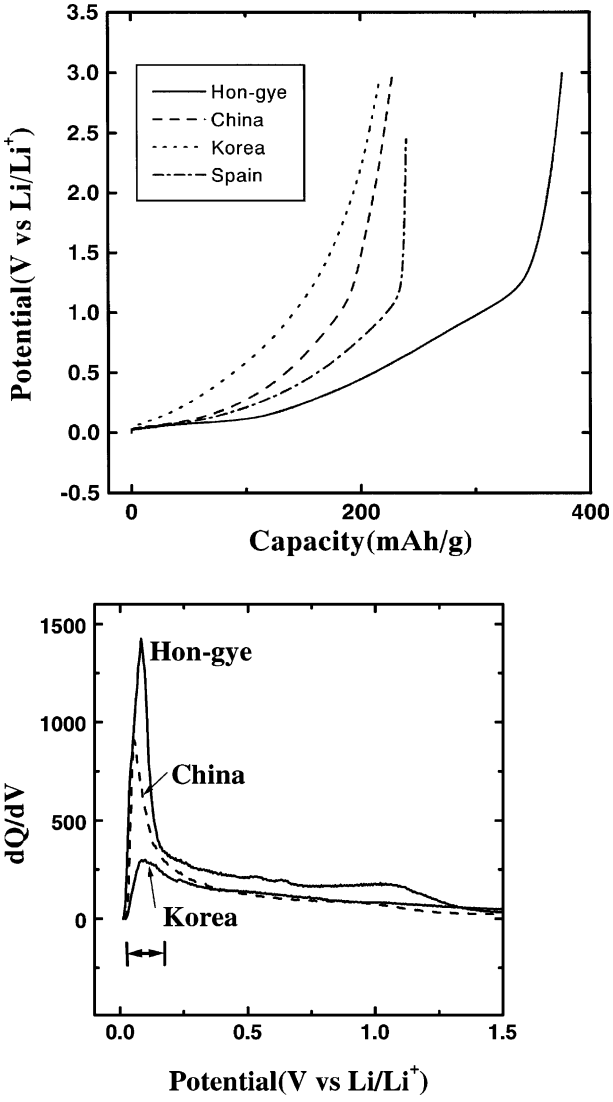

Fig. 8. Discharge profiles of various anthracite, CC–CV (charge: 30 mA/g to 0 V and at 0 V for 6 h, discharge: 30 mA/g to 2 V).

minerals. South Korea and China anthracites were indicated to carry SiO_2, SiO_2 and Illite, respectively. Fig. 9(b) shows that the width of carbon peaks at 25° increased in the order of China, South Korea, Spain, and Hon-gye anthracites which were heat-treated at 1100 °C. 2θ of the peaks decreased in the order of China, South Korea, Spain, and Hon-gye anthracites.

3.4. TEM observation of anthracites

Fig. 10 illustrates TEM images of Hon-gye anthracite calcined up to 1800 °C in terms of their stacking layers. As-received Hon-gye anthracite shows spherical bedding of aromatic sheets. Random orientation among spheres was observed and it showed basic anisotropic due to overall arrangement as reported by Oberlin and Terriere [30]. Carbonization flattened the spheres, indicating growth of

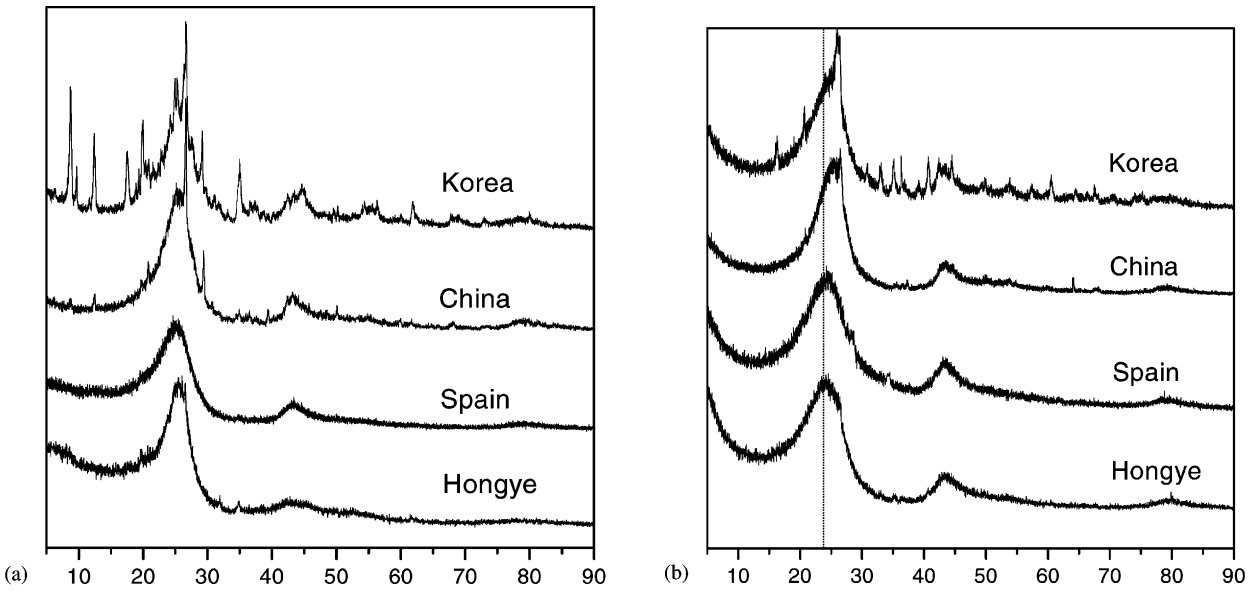

Fig. 9. Powder X-ray diffraction patterns of various anthracites (a) as-received (b) heat-treated at 1100 °C.

planes. Large voids are formed, however, no microvoid was observed. Calcination at 1050 °C induced microvoids among microclusters of graphite. Calcination at 1800 °C reduced the numbers of microvoids and clusters since the graphitization enlarged the graphene sheets and their stacking, reducing the number of microclusters to remove microvoids among the microclusters.

China anthracite calcined at 1100 °C showed a similar image (Fig. 11) with that of Hon-gye anthracite calcined at 1800 °C (Fig. 10), indicating early graphitization.

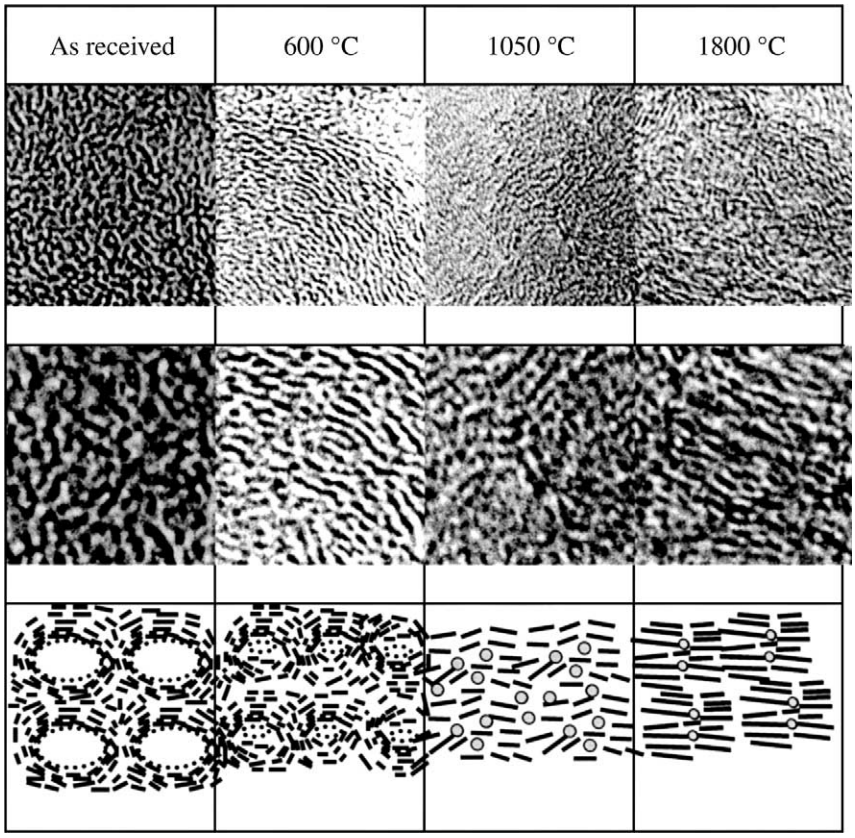

Fig. 10. TEM images of Hon-gye anthracite heat-treated at various temperatures (the first line: 3,200,000×; the second line: their magnified images; the third line: structural models).

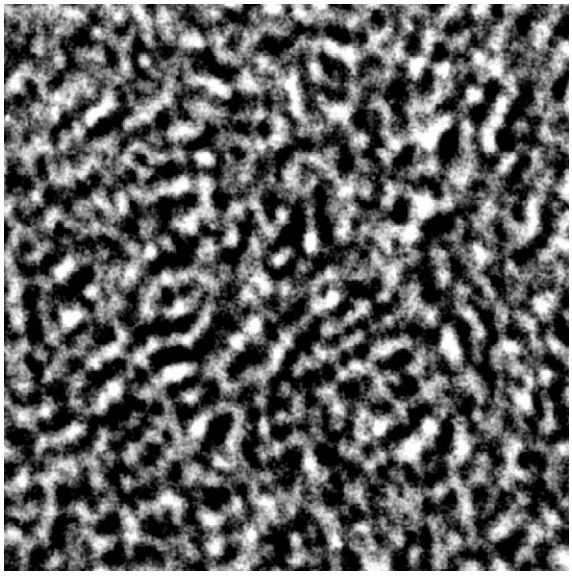

Fig. 11. TEM images of China anthracite heat-treated at 1100 °C.

4. Discussion and conclusion

This experiment confirmed following two points of anthracites, particularly Hon-gye coal as anodic carbon material for the lithium ion secondary battery.

1. Unique carbonization behaviors of anthracite to give characteristic features of graphitizable, non-graphitizable, and graphitic carbons.
2. Anthracite can be a promising candidate for anodic material of the next generation in terms of high capacity and rapid charge–discharge as the non-graphitic.

The storage sites of carbons have been summarized according to the extensive studies [13,16,17,31,32]. There are five sites:

Site I: charge–discharge at 0.12–0.8 V;
Site II: charged at 0–0.1 V to discharge at 1 V;
Site III: charged at 0–0.1 V to discharge at 0.1 V;
Site IV: charge–discharge at 0–0.13 V;
Site V: irreversible charging sites.

Site I is identified to the graphene layers. The growth of graphite crystal governs the extent of intercalation, from higher stage to the first stage C_6Li through several stages. Stages of intercalation are also governed by the charge potential to show staged charge and discharge. Thus, such charge–discharge profiles are characteristic to the graphite.

Less uniformity of graphitization provides more cluster of different graphite stacking, which allows a series of sites of charge and discharge potentials. Charge and discharge at continuous variation of potentials, were observed at 0–0.1 and 1 V, respectively. Thus, site II is a group of storage sites around graphene sheets of very variable stacking, including their surface.

Site III stores highly reduced lithium ions which are believed to be located in the microvoids. The internal surface of microvoid can stabilize such ions through charge transfer. A cluster of lithium ions in a microvoid allows their exchange to share the stabilization.

The highly reduced lithium ion can be also stored at site IV, the microvoid surrounded by the hexagonal plane of graphene, to be discharged at 0–0.13 V probably with some chemical change at the edge. Hence, the cycle stability is usually poor.

Site V stores the irreversible charge, being observed basically at 0.8 V (site V_1) and 0.1 V (site V_2) of charge. First site reflects the formation of solid electrolyte interface (SEI) film which captures lithium ion to be excluded in the further electrochemical redox. The second site is ascribed to the reactivity of highly reduced ion with impurity in the carbon.

The anthracite heated at 600–900 °C was found to show anodic performances relying upon all of the above sites which vary their contribution markedly according to the heat-treatment temperatures. Heating up to 1100 °C emphasized the non-graphitic natures of anthracite, increasing markedly discharge at site III. Graphitizable sites are minimized while site IV disappears. Above 1600 °C, graphitization started sharply to emphasize staged charge–discharge which is characteristic to that of the graphite. Higher temperature of heat-treatment increases the extent of graphitization. Ash minerals, oxygen and some of graphene edge may be site V_2. The latter two sites can be removed by higher heat-treatment. The lowest oxygen content of anthracite among the carbon can be good news.

Among the anthracites examined in the present study, Hon-gye anthracite is the best one. Moderate size of its graphene clusters and their deformability may form by the heat-treatment and a number of micropores surrounded by small clusters chained in a circle. Low content of ash minerals which decreases with HTT probably because of decomposition of some component is another advantage of Hon-gye. As a result, Hon-gye calcined at 1100 °C showed the reversible capacity of 200 mAh/g at 0.3 V. Such a characteristic performance of non-graphitic carbon must be noted. Its high density of 1.43 g/cm^3 is an advantage for high capacity per volume. Optimization of particle size, heating conditions to optimize volatilization and graphitization extent, and removal of oxygen, and large voids may further improve its performance. Removal of minerals may form voids in the coal particle, microporous not mesoporous void being expected to be introduced. Mesoporosity can be minimized by optimization of the particle size.

In conclusion, the anthracite shows the reasonable reversible capacity of 370 mAh/g, in addition, its simple process to prepare an active material and low cost of coal are attractive for its application to lithium ion battery. The anthracite coke is considered as one of the hard carbons from view of the electrochemical behaviors. The anodic performance of anthracite depends upon its microstructure,

and non-graphitic alignment of the smallest hexagon stacking is necessary for higher capacity at low voltage.

References

[1] T. Nagaura, T. Tozawa, Prog. Battery Solar Cells 9 (1990) 20.
[2] J.R. Dahn, A.K. Sleigh, H. Shi, B.M. Way, W.J. Weydanz, J.N. Reimers, Q. Zhong, U. von Sacken, in: G. Pistoia (Ed.), Lithium Batteries: New Materials, Development and Perspectives, Elsevier, London, 1995, p. 1.
[3] R. Fong, U. von Sacken, J.R. Dahn, J. Electrochem. Soc. 137 (1990) 2009.
[4] J.R. Dahn, T. Zheng, Y. Liu, J.S. Xue, Science 270 (1995) 590.
[5] A. Mabuchi, K. Takumitsu, H. Fujimoto, T. Kasuh, J. Electrochem. Soc. 142 (1995) 1041.
[6] N. Takami, A. Satoh, M. Hara, T. Ohsaki, J. Electrochem. Soc. 142 (1995) 2564.
[7] T. Iijima, K. Suzuki, Y. Matsuda, Synth. Met. 73 (1996) 9.
[8] T. Ohzuku, Y. Iwasashi, K. Sawai, J. Electrochem. Soc. 140 (1993) 2490.
[9] Z.X. Shu, R.S. McMillan, J.J. Murray, J. Electrochem. Soc. 140 (1993) 922.
[10] T.D. Tran, L.M. Spellman, W.M. Goldberger, X. Song, K. Kinoshita, J. Power Sources 68 (1997) 106.
[11] R. Kostecki, T.D. Tran, X. Song, K. Kinoshita, F. McLarnon, J. Electrochem. Soc. 144 (1997) 3111.
[12] M. Jean, A. Tranchant, R. Messina, J. Electrochem. Soc. 143 (1996) 391.
[13] N. Sonobe, M. Ishikawa, T. Iwasaki, in: Proceedings of the 35th Battery Symposium, Japan, November 14–16, 1994, p. 47.
[14] J.R. Dahn, A.K. Sleigh, H. Shi, J.N. Reimers, Q. Zhong, B.M. Way, Electrochim. Acta 38 (1993) 1179.
[15] A. Gibaud, J.S. Xue, J.R. Dahn, Carbon 34 (1996) 499.
[16] K. Sato, M. Noguchi, A. Demachi, N. Oki, M. Endo, Science 264 (1994) 556.
[17] Y. Takahashi, J. Oishi, Y. Miki, M. Yoshimura, K. Shibara, H. Sakamoto, in: Proceedings of the 35th Battery Symposium, Japan, November 14–16, 1994, p. 14.
[18] D. Aurbach, Y. eia-Eli, O. Chusid, Y. Carmeli, M. Babai, H. Yamin, J. Electrochem. Soc. 141 (1994) 603.
[19] K. Tokumitsu, A. Mabuchi, H. Fujimoto, T. Kasuh, J. Electrochem. Soc. 143 (1996) 2235.
[20] Y. More, T. Iriyama, T. Hashimoto, S. Yamazake, F. Kawakami, H. Shiroki, T. Yamabe, J. of Power Sources 56 (1995) 205.
[21] T. Zheng, W. Xing, J.R. Dahn, Carbon 34 (1996) 1501.
[22] Y. Chang, H. Sohn, Y. Korai, I. Mochida, Carbon 36 (1998) 1653.
[23] R.C. Bansal, J.B. Donnet, F. Stoeckli, Active Carbon, Marcel Dekker, New York, 1988, pp. 121–129.
[24] P.L. Walker, A. Almargo, Carbon 33 (1995) 239.
[25] G.A.R. Bessant, P.L. Walker, Carbon 32 (1994) 1171.
[26] M.C. Mittelmeijer-Hazeleger, J.M. Martin-Martinez, Carbon 30 (4) (1992) 695.
[27] M.J. Munoz-Guillena, M.J. Illan-Gomes, J.M. Martin-Martinez, A. Linares-Solano, C. Salinas-Martinez de Lecea, Energy Fuels 6 (1) (1992) 9.
[28] J.B. Parra, J.J. Pis, J.C. Sousa, J.A. Pajares, R.C. Bansal, Carbon 34 (6) (1996) 783.
[29] R.E. Franklin, Proc. R. Soc. 209 (1951) 196.
[30] A. Oberlin, G. Terriere, Carbon 13 (1975) 367.
[31] C.W. Park, S.-H. Yoon, S.I. Lee, S.M. Oh, Carbon 38 (2000) 995.
[32] I. Mochida, C.-H. Ku, Y. Korai, Carbon 39 (2001) 399.